Central European Journal of Energetic Materials, **2014**, *11*(2), 199-218
ISSN 1733-7178

Investigation of the Cook-off Processes of HMX-based Mixed Explosives

Lang CHEN, Xin MA*, Feng LU and Junying WU

State Key Laboratory of Explosion Science and Technology, Beijing Institute of Technology, Beijing100081, China
**E-mail: maxin0926@hotmail.com*

Abstract: In order to investigate the characteristics of the thermal reaction for two kinds of mixed explosives, PBXC-10 (HMX/TATB/Binder, 38/57/5) and JO-8 (HMX/Binder, 95/5), multi-point measured temperature cook-off tests were carried out at different heating rates. The thermal transfer and finite chemical reactions that include the $\beta \rightarrow \delta$ transition of HMX, and the endothermic and exothermic cook-off processes were analyzed. A 3D model of the explosive cook-off test was developed to simulate the thermal and chemical behaviour in a thermal ignition. The decomposition mechanisms for HMX and TATB are described by the multistep, chemical kinetic model. The thermal properties, decomposition pathways, and chemical kinetic reaction rate constants for each component are used to develop the reaction courses at various weight percentages. The thermal decomposition reaction of a multi-component, mixed explosive can be predicted as long as the chemical kinetics model of each single-base explosive and binder are known. The phase transition of HMX has an influence on the temperature of the explosive, especially for an explosive with a high HMX content. For mixed explosives containing HMX and TATB, most of the heat release is produced by the decomposition of HMX before ignition, but TATB can delay the ignition time and decrease the reaction violence in the cook-off process.

Keywords: explosives, chemical kinetics, thermal decomposition, cook-off, numerical simulation

1 Introduction

The cook-off test is one of the main methods for studying the safe handling of explosives and for examining chemical kinetic models for high explosives. From a cook-off experiment, the ignition time and reaction violence of an energetic material can be obtained to confirm its criticality. On the other hand, there is great interest in using computer simulations to predict the heating process of an explosive.

A series of experiments exists which are designed to study the thermal processes of an explosive. The one-dimensional time-to-explosion (ODTX) test is used to study the thermal sensitivity and thermal explosion of energetic materials [1]. In the ODTX test, the explosive is heated at a constant temperature until ignition. It can measure the ignition times, the lowest explosion temperatures and evaluate the violence of a thermal explosion of an energetic material [2]. It can also be used to calibrate the parameters of chemical kinetic models of explosives [3]. However the detailed temperature distribution inside the explosive cannot be obtained in the ODTX test. The small-scale cook-off bomb (SCB) test is used to simulate the situation during transport and storage of explosives when subjected to thermal stimuli [4, 5]. In a SCB experiment, the explosive is sealed into a steel casting and heated at different heating rates until ignition. There are some difficulties in displaying the variations in temperature because only a few thermocouples can be inserted into the explosive. A scaled thermal explosion (STEX) experiment provides qualitative indication of the violence of the response from thermal stimuli through fragment analysis of the steel case [6]. In many cases, most cook-off experiments employ only external thermocouples that do not permit insight into the details leading to ignition. A Sandia instrumented thermal ignition (SITI) experiment can investigate the process of thermal ignition, which is accomplished by embedding a grid of thermocouples between two pellets of explosives [7]. This increases the accuracy of the temperature measurement and reduces the impact of the thermocouples on the structure of the explosive.

Many groups have attempted to develop simulation models for the response of explosives exposed to increasing temperatures, which requires more detail of the thermal decomposition of the explosive. Semenov used a zero-order single-rate expression to describe the exothermic decomposition of explosives and calculated the critical temperature and ignition time for the first time [8]. However, his theory assumed that the temperature in the whole reactant was uniform and this assumption was not suitable for solid explosives. This shortcoming was overcome by Frank-Kamenetskii, who considered heat conduction theory under non-uniform temperature conditions [9]. The Frank-Kamenetskii theory is closer to reality.

However in these theories it was generally assumed that the major pathway for explosive decomposition was from the reactant to the final stable gas products in a single step, largely neglecting the influence of intermediates. In reality, there is a close relationship between the thermal process of the cook-off and the components in the explosive, and it has been demonstrated that a single-rate expression cannot describe the reaction of each component or predict the cook-off process of a multi-component mixed explosive. McGuire and Tarver published a chemical decomposition model that included three step kinetic expressions and calculated the explosion times for the pure explosives HMX, TATB, RDX and TNT [10]. The multi-step kinetic model is successful in considering the intermediates in the reaction, describing the thermal process of the explosive and building the foundation for models and numerical strategies for the thermal behavior of explosives. Tarver *et al*. developed new PBX chemical decomposition models that include cross-reactions between gaseous explosive products and binders, and accurately predicted the ODTX time to explosion [11, 12]. Yoh *et al*. used an arbitrary Lagrangian-Eulerian (ALE3D) code that modelled the heating, ignition, and deflagration phases for RDX and HMX [13, 14]. Dickson *et al*. developed a four-step model that included transition state theory (TST) kinetics to represent the nucleation and growth process of the transition of HMX [15]. Perry *et al*. presented a four-step reversible kinetic model for HMX and accurately predicted the timing and temperature behaviour for the cook-off process and the impact-induced friction ignition problem [16]. Presently, computer simulations are being developed for investigating more widely the cook-off process [17, 18]. However most of the recent modelling efforts have been focused on single-base explosives and do not consider the effect of components in mixed explosives. The details of the relatively slow heating phase of a mixed explosive and methods for dealing with each component was largely neglected in these calculation studies. Thus, there is great interest in studying the thermal safety of multi-component mixed explosives.

In this paper, two kinds of mixed explosives, namely PBXC-10 (HMX/TATB/Binder, 38/57/5) and JO-8 (HMX/Binder, 95/5), have been investigated using the multi-point measured temperature cook-off test at different heating rates. The thermal reaction states of the explosives were analyzed by measuring the temperature at different locations in the explosive charge. The multistep chemical kinetics model was used to describe the chemical decomposition of HMX and TATB respectively. A multi-component grid calculation method was established to calculate the heat of reaction of each component during the cook-off process. The influences of component content on the cook-off process have been analyzed.

2 Experiment

The multi-point measured temperature cook-off test system, which is similar in many respects to the Sandia instrumented thermal ignition (SITI) [7], was designed. Figure 1 shows a schematic diagram of the cook-off test device. The setup consists primarily of two steel shells and two pellets of energetic material. The cook-off bomb consists of an upper and a lower component, each part having a steel shell and an explosive pellet. Each explosive pellet has a diameter of 50 mm and a height of 25 mm, giving a total height of 50 mm (see Figure 1). There are expansion gaps, 44 mm in diameter and 2 mm in depth, adjacent to each pellet allowing for volumetric expansion of the energetic material during heating while maintaining compression between the two pellets. Seven type K thermocouples, typically 0.08 mm in diameter, are embedded between the two pellets. The pellets are then confined by steel shells which are pressed together with 4 bolts. High temperature sealant bond is coated between the two shells. Heating is provided by a ceramic heater wrapped around the steel cylinders and controlled by a NOVA 300 series digital controller, with the control thermocouple between the heater and the steel. Figure 2 shows the upper and lower parts of the cook-off bomb before assembly. Figure 3 shows the arrangement of thermocouples. The thermocouples are labeled TC1-TC7 with increasing radial distance from the center. Figure 4 shows a photograph of the cook-off bomb assembled for a test.

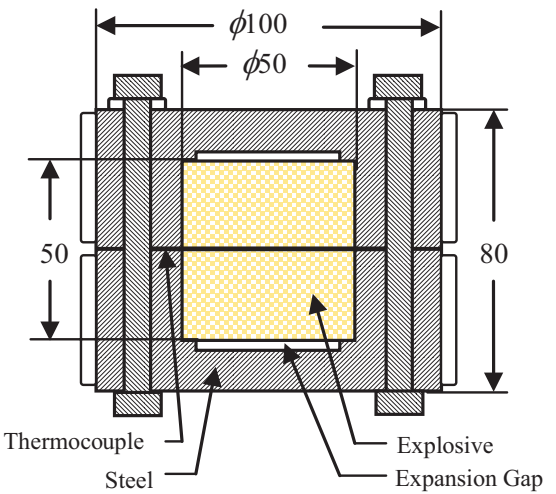

Figure 1. Schematic of the geometry of the cook-off test.

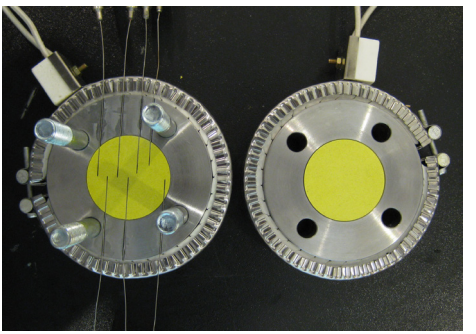

Figure 2. Photograph of the upper and lower parts of the cook-off bomb before assembly.

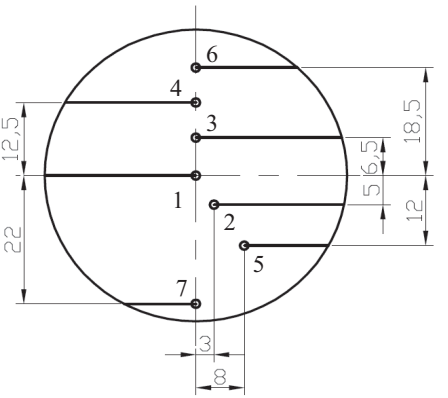

Figure 3. Arrangement of the thermocouples.

Figure 4. Photograph of the upper and lower parts of the cook-off bomb after assembly.

Five different heating rates were employed during the cook-off tests of PBXC-10, 9.1, 5.0, 1.1, 0.8 and 0.5 $K \cdot min^{-1}$, respectively. JO-8 was heated at two constant temperature ramp rates, typically 2.2 and 2.7 $K \cdot min^{-1}$, until an explosion occurred. The thermocouple signals were recorded by a HIOKI 8432 data logger.

2.1 Numerical simulation

In the cook-off test, the heat of the environment is transferred from the outside to the inside of the explosive. In this modelling work, we wanted to reproduce the internal temperature profiles observed in the cook-off test. The single-rate kinetic mechanism was calculated simply and saves time and cost. However many previous studies proved that the single-rate expression cannot provide accurate spatial or timing details of slow cook-off ignition. Therefore we chose a multistep chemical kinetic model to describe the decomposition mechanisms of HMX and TATB. Chemical decomposition reactions for each component of the explosive, such as HMX, TATB and binders, take place. As the exothermic reaction occurs, self-heating tends to cause acceleration in the reaction rate until explosive ignition. It is necessary to describe the chemical decomposition of each component in a mixed explosive in order to model the cook-off process. Single based explosives, such as HMX and TATB, can be described by a multistep chemical kinetic model, and the cross-reactions between gaseous explosive products and binders can be considered. During the decomposition phase of each component, exothermic and endothermic reactions will occur simultaneously, the whole heat of the reaction being the sum of the exothermic and endothermic reactions.

The four-step, three-species reaction mechanism for HMX, which was developed by Perry *et al*. [16], was used as follows:

$$\text{A}\rightarrow\text{B}, \qquad r_1 = \frac{kT}{h}\exp\left(\frac{T\Delta S_{1f} - E_{1f}}{RT}\right)\rho_A - \frac{kT}{h}\exp\left(\frac{T\Delta S_{1r} - E_{1r}}{RT}\right)\rho_B \tag{1}$$

$$\text{A+B}\rightarrow\text{B}, \quad r_2 = \frac{kT}{h}\exp\left(\frac{T\Delta S_{2f} - E_{2f}}{RT}\right)\rho_A\rho_B - \frac{kT}{h}\exp\left(\frac{T\Delta S_{2r} - E_{2r}}{RT}\right)\rho_A\rho_B \tag{2}$$

$$\text{B}\rightarrow\text{C}, \qquad r_3 = Z_3 \exp(-E_{f3}/RT)\rho_B \tag{3}$$

$$\text{B+C}\rightarrow\text{C}, \quad r_4 = Z_4 \exp(-E_{f4}/RT)\rho_B\rho_C \tag{4}$$

where A and B are solid species (β-HMX and δ-HMX), C is the products; ρ_A, ρ_B and ρ_C represent the mass fractions of β-HMX, δ-HMX and products respectively; r is the mass reaction rate; Z is the frequency factor, and E is the activation

energy; ΔS is the activation entropy for the reactions; k is Boltzmann's constant; h is Planck's constant; R is the molar gas constant. The associated parameters for each rate equation are shown in Table 1.

We used a combination of unimolecular and bimolecular forms of the thermodynamic formulation of conventional transition state theory (TST) kinetics to represent the nucleation and growth processes of the transition, which is provided by Henson *et al*. [19]. After the sharp phase transition, comparison with heat-transfer code predictions indicated that a slow endothermic process occurs. A first order Arrhenius step was used to model this. Finally, a bimolecular exothermic reaction leads to thermal runaway.

The reaction mechanism for TATB , which was developed by Tarver *et al*. [11], was used as follows:

$$\mathrm{F}\rightarrow\mathrm{G}+\mathrm{H_2O}, \quad r_5 = Z_5 \exp(-E_5 / RT)\rho_F \tag{5}$$

$$\mathrm{G}\rightarrow\mathrm{H}+\mathrm{Gases}, \quad r_6 = Z_6 \exp(-E_6 / RT)\rho_G \tag{6}$$

$$\mathrm{H}\rightarrow\mathrm{I}, \quad r_7 = Z_7 \exp(-E_7 / RT)\rho_H^2 \tag{7}$$

where F is TATB, G and H are solid intermediates, and I is the final gas products, respectively; ρ_F, ρ_G and ρ_H represent the mass fractions of TATB, G and H, respectively. The associated parameters for each rate equation are shown in Table 2.

Kel-F is an endothermic binder, and is more thermally stable than HMX and TATB [12]. The binder is assumed to decompose according to a simple first order reaction:

$$\mathrm{J}\rightarrow\mathrm{K}, \quad r_8 = Z_8 \exp(-E_8 / RT)\rho_J \tag{8}$$

where J is Kel-F, and K is the decomposition products.

Reaction (8) is assumed to be an endothermic, first-order reaction. Kel-F contains C-H, C-Cl, and C-F bonds, and TATB decomposition produces intermediate species such as HCN, CO, CO_2, HNCO, and NO, which can react with the polymer bonds [20]. So for TATB, the final gaseous products generated in the reactions represented by reaction (9) are assumed to react with the binder:

$$\mathrm{I}+\mathrm{J}\rightarrow\mathrm{L}, \quad r_9 = Z_9 \exp(-E_9 / RT)\rho_I\rho_J \tag{9}$$

where I is the final gaseous products, J is Kel-F, and L are the fragments, respectively; ρ_I and ρ_J represent the mass fractions. The associated parameters for each rate equation are shown in Table 3. Additionally, we do not consider

the reaction between HMX and Kel-F, because no chemical kinetic rate data are available yet.

Tables 1 and 2 list the chemical kinetics parameters for the HMX and the TATB decomposition models, respectively. Most of these parameters are the same as in previous literature [12, 17], but No. 4 Z and No. 4 ΔS_f have been modified slightly to improve the agreement with experiment. Table 3 lists the Kel-F and cross-reaction parameters. Table 4 lists the parameters for HMX, TATB and Kel-F [21]. The specific heat and thermal conductivity of the mixed explosives are mass fraction weighted with the thermal properties for each species.

Table 1. Chemical kinetic parameters for HMX

No.	Z [s^{-1}]	ΔS_f [$J \cdot mol^{-1} \cdot K^{-1}$]	E_f [$J \cdot mol^{-1}$]	ΔS_r [$J \cdot mol^{-1} \cdot K^{-1}$]	E_r [$J \cdot mol^{-1}$]	Q [$kJ \cdot kg^{-1}$]
1	…	123	2.040 E5	89.0	1.890 E5	-25
2	…	-40[a]	1.015 E5	-75.2	8.650 E5	-25
3	3.16E16	…	2.000 E5	…	…	-120
4	3.50E15 [b]	…	1.731 E5	…	…	3200

[a] -40 for PBXC-10 and -41.7 for JO-8;
[b] 3.50 E15 for PBXC-10 and 9.0 E14 for JO-8.

Table 2. Chemical kinetic parameters for TATB

No.	Z [s^{-1}]	E [$J \cdot mol^{-1}$]	Q [$kJ \cdot kg^{-1}$]
5	7.0167E20	252000	-210
6	8.7493E12	176400	-210
7	4.356E11	141960	2940

Table 3. Chemical kinetic parameters for Kel-F and cross-reactions

No.	Z [s^{-1}]	E [$J \cdot mol^{-1}$]	Q [$kJ \cdot kg^{-1}$]
8	9.9349E17	272328	-5871.6
9	7.6948E23	272328	-2520

Table 4. Parameters for HMX, TATB and Kel-F

Material	Density [$kg \cdot m^{-3}$]	Heat capacity [$J \cdot kg^{-1} \cdot K^{-1}$]	Thermal conductivity [$W \cdot m^{-1} \cdot K^{-1}$]
HMX	1850	1050	0.345
TATB	1835	1170	0.544
Kel-F	2020	1004	0.0005

The three-dimensional calculation model was established according to the cook-off diagram, shown in Figure 5. The model domain is a symmetrical cylinder. A quarter model of the domain was set up to decrease computing time. The model mainly includes the explosive cylinder, the steel vessel and the air gap. The radiation of heat in the air gap was also considered. In the simulations, the mesh elements were considered as multicomponent elements which contain both explosives and binders. The decomposition of each component was modeled by a multistep chemical kinetics model. The whole heat of each element is the sum of both endothermic and exothermic elements for each component.

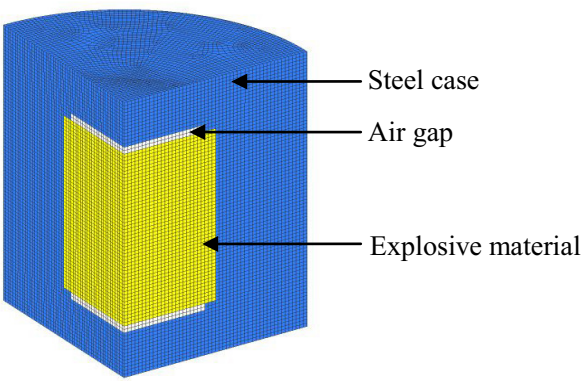

Figure 5. Calculation grid for the model.

In Cartesian coordinates, the energy equations is:

$$\rho c_P \frac{\partial T}{\partial t} = \lambda \frac{\partial}{\partial x}\left(\frac{\partial T}{\partial x}\right) + \lambda \frac{\partial}{\partial y}\left(\frac{\partial T}{\partial y}\right) + \lambda \frac{\partial}{\partial z}\left(\frac{\partial T}{\partial z}\right) + S \tag{10}$$

Here, ρ is the density, and S is the heat source term for the explosive decomposition reaction.

The numerical simulation was performed by the Computational Fluid Dynamics(CFD) software, Fluent. The boundary condition was treated as the heated boundary in this simulation. The heat source and the heating rate are written as user defined subroutines by C language and then imported into the software. Based on the chemical kinetics model of each single explosive, such as HMX and TATB, and with the multicomponent grid unit calculation method, the thermal decomposition of mixed explosives can be calculated directly.

3 Results and Discussion

Experimental

Figure 6 shows a post-ignition photograph from a PBXC-10 cook-off test at a heating rate of 1.1 $K \cdot min^{-1}$. The photograph indicates that the confining steel almost kept its integrity although the shells had been opened. There was a small amount of black residue in the shell and unreacted yellow powder around the vessel. It can be seen that explosion did not occur in the PBXC-10 explosive, just incomplete combustion. Figure 7 shows the temperatures measured with the internal thermocouples from the experiment at a heating rate of 1.1 $K \cdot min^{-1}$. As seen from Figure 7A, TC7 measures the temperature close to the edge of the explosive, which is always higher than other thermocouple temperatures. The other thermocouple temperatures were nearly the same because of the slow heating rate. After about 10000 s (2.78 hours), a temperature flat appeared in TC5, TC4, TC2 and TC1 in turn, as shown in Figure 7B. This is caused by the β→δ endothermic phase transition. The equilibrium phase transition temperature between β-HMX and δ-HMX is at about 442 K, and the transition appeared to commence around 439 K and lasted until 446 K in this experiment. However the β→δ transition in the overall cook-off process affected the temperature distribution in only a small way because PBXC-10 contains only 38% HMX. Otherwise this does not appear in TC7, because it is closest to the edge of the explosive, and is mainly affected by the external heating.

Figure 6. Post-ignition photograph.

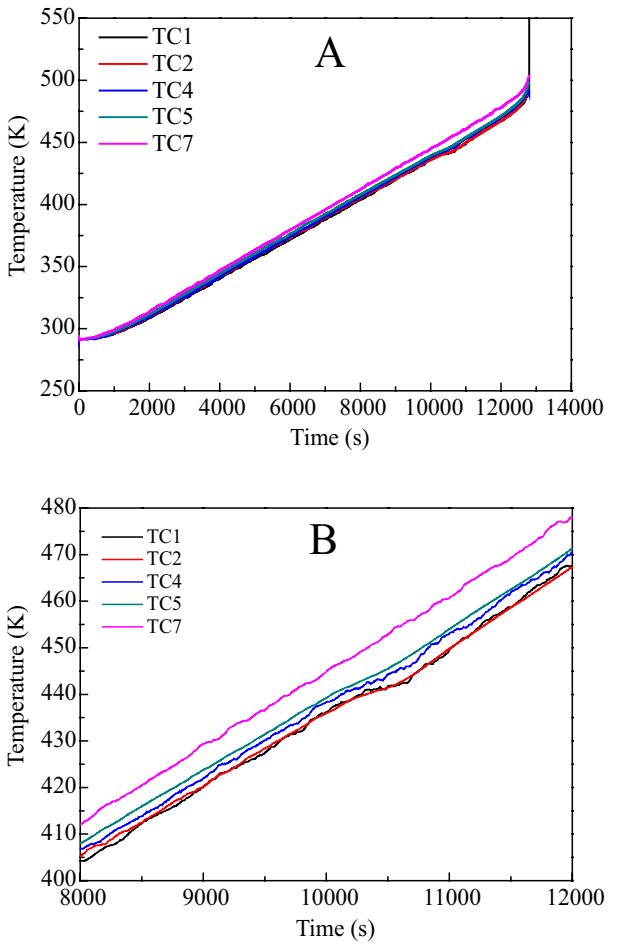

Figure 7. Measured temperatures from different thermocouples from the PBXC-10 cook-off test. Cook-off test data (A) 0-14000 s, (B) 8000-12000 s.

The ignition time of PBXC-10 and the shell temperature at ignition at different heating rates are summarized in Table 5. From Table 5, the ignition time was 1884 s (0.53 hours) and the shell temperature was 571 K at a heating rate of 9.1 $K \cdot min^{-1}$. The ignition time was 17488 s (4.86 hours) and the shell temperature was 494 K at a heating rate of 0.5 $K \cdot min^{-1}$. The results show that the ignition time is increased and the shell temperature is decreased as the heating rate is decreased.

Table 5. Ignition time of explosive and shell temperature at ignition for different heating rates of PBXC-10

No.	Heating rate [K·min^{-1}]	Ignition time [s]	Shell temperature [K]
1	9.1	1884	571
2	5.0	3167	549
3	1.1	12801	519
4	0.8	14490	510
5	0.5	17488	494

The measured point temperatures at ignition for the different heating rates are summarized in Table 6. The temperature of TC7 (22 mm from the explosive center) is the highest when the explosive ignites at heating rates of 9.1, 5 and 1.1 K·min^{-1}. The temperature of TC5 (14.42 mm from the explosive center) is the highest when the explosive ignites at a heating rate of 0.8 K min^{-1}. The temperature of TC1 (in the center of the explosive) is the highest when the explosive ignites at a heating rate of 0.5 K min^{-1}. With lower heating rates, the high-temperature region is gradually moving to the center of the explosive, as is the ignition location.

Table 6. Measured point temperatures at ignition for different heating rates of PBXC10

Heating rate [K·min^{-1}]	TC1 temperature [K]	TC2 temperature [K]	TC3 temperature [K]	TC4 temperature [K]	TC5 temperature [K]	TC6 temperature [K]	TC7 temperature [K]
9.1	422	429	427	441	453	470	504
5.0	450	454	454	464	471	481	503
1.1	491	491	----	489	497	----	503
0.8	----	487	485	486	490	488	486
0.5	521	506	-----	495	506	----	503

Two experiments were performed with JO-8 explosive. By studying the fragments of the shell, it can be concluded that explosion of JO-8 had occurred. These experiments are summarized in Table 7. The results show that the ignition time is increased as the heating rate is decreased. However the shell temperatures at ignition are little changed at these two heating rates.

Table 7. Ignition time of explosive and shell temperature at ignition at different heating rates of JO-8

No.	Heating rate [K·min^{-1}]	Ignition time [s]	Shell temperature [K]
1	2.2	6426	536
2	2.7	5135	539

4 Calculation

Table 8 shows the experimental and calculated ignition times, and shell temperatures at different heating rates. It is seen that there is good agreement, with a maximum difference of 7.5% between the experimental and simulation results, for the ignition time and the temperature of the shell when ignition occurred.

Table 8. Measured and calculated ignition time and shell temperature

Material	Heating rate [K·min^{-1}]	Time [s]			Shell temperature [K]		
		Experiment	Simulation	Difference [%]	Experiment	Simulation	Difference [%]
PBXC-10	9.1	1884	1940	2.97	571	581	1.75
PBXC-10	5.0	3167	3159	0.25	549	548	0.18
PBXC-10	1.1	12801	12777	0.18	519	518	0.19
PBXC-10	0.8	14490	14447	0.30	510	509	0.20
PBXC-10	0.5	17488	18158	3.83	494	499	1.01
JO-8	2.2	6426	5958	7.28	536	544	1.49
JO-8	2.7	5135	5211	1.48	539	538	0.19

Figure 8 shows the calculated ignition location at a heating rate of 1.1 K·min^{-1} for PBXC-10 explosive, which appears as circles on the top and bottom of the energetic material. This figure is obtained using the Ansys CFD-Post software. The shell temperature was higher than the internal temperature of the explosive until ignition, and heat flows from the external source to the internal part of the explosive. Figure 9 shows the experimental and calculated temperature versus time curves for TC1 and TC7. This figure is obtained using the OriginPro software. These data, associated with phase transition, agree with the experimental results. The measured ignition time was 12801 s (3.56 hours) when the temperature of TC1 was 491.2 K and TC7 was 502.9 K. The calculated ignition time was 12777 s (3.55 hours) and the ignition temperature of TC1 was 481.3 K and TC7 was 495.3 K. Therefore the agreement between

calculated and measured results demonstrates that the cook-off model and the relevant parameters can accurately describe the decomposition of HMX, TATB and Kel-F.

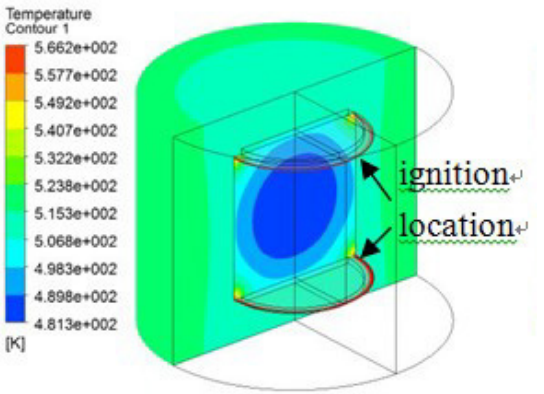

Figure 8. Calculated ignition location for PBXC-10.

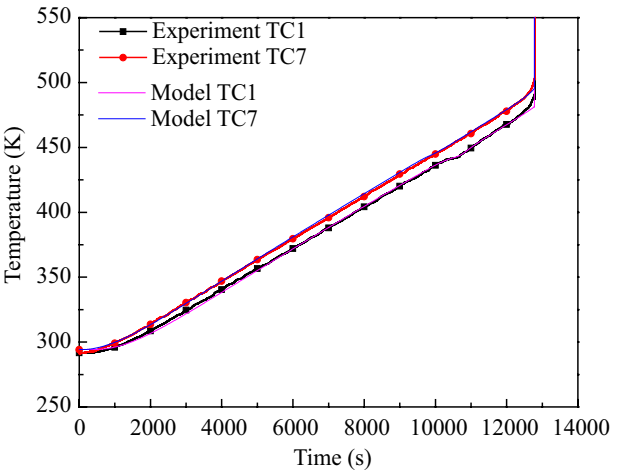

Figure 9. Measured and calculated T-t curves for PBXC-10.

Figure 10 shows the calculated ignition location at a heating rate of 2.2 $K \cdot min^{-1}$ for JO-8 explosive, which appears as circles on the top and bottom of the energetic material, as for PBXC-10. Figure 11 shows the temperature profiles for TC1 and TC7, comparing computational and experimental data. It is clear that the computational model prediction for TC7 matches the experimental data well.

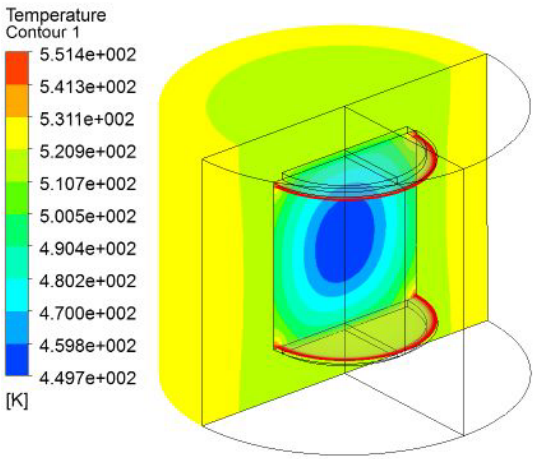

Figure 10. Calculated ignition location for JO-8**.**

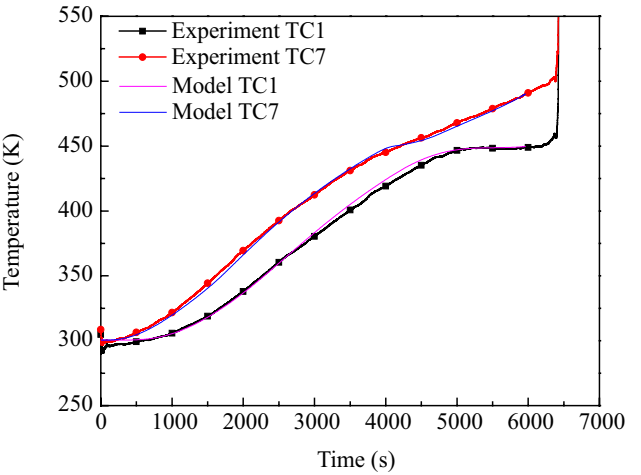

Figure 11. Measured and calculated T-t curves for JO-8.

For TC1, the explosive commenced the β→δ phase transition at 448 K, but the predicted temperature is higher than the experimental data from 2750 s (0.76 hours) until explosion occurred. The cause of this is that the phase transition results in changes in some of the parameters (density, thermal conductivity, viscosity, *etc*.), influencing the temperature field of the explosive. Therefore, it is important to obtain accurate input parameters for a perfect simulation of the phase transition and the temperature field in the explosive. The measured

ignition time was 6426 s (1.79 hours) and the calculated ignition time was 5958 s (1.66 hours), an error of 7.28%. Therefore the agreement between calculated and measured results demonstrates that the cook-off model and the relevant parameters can accurately describe the phase transition and the decomposition of HMX. The results for experiments with JO-8 and PBXC-10 indicated that the temperatures of the phase transition of HMX are different. The flat temperature of PBXC-10 is 441 K and 448 K for JO-8. Cook-off data are sensitive to the type of explosive used. There are many factors affecting the flat temperature, such as the quality of the crystal (density, shape, *etc*.) and the type of solid binder.

Figure 12 shows the mass fraction of each component at the ignition location during the process of cook-off. For PBXC-10 (Figure 12A), it can be seen that β-HMX consumption is fast, causing a steep increase of the δ-HMX signal, as the temperature increases up to 441 K. The much slower δ-HMX consumption is initiated by the decomposition reaction, so that the final products' signal is increasing slowly. As the temperature increases, the consumption of δ-HMX is also accelerated and more final products are created. However, TATB and Kel-F consumptions are small before ignition. Ignition did not occur until the temperature reached 566 K. This demonstrated that the heat released by the decomposition reaction of HMX is mostly before ignition. For JO-8 (Figure 12B), which is mostly HMX (95%), there is a similar mechanism as for PBXC-10. The calculated results show that β-HMX is converted rapidly to δ-HMX when the temperature gets above 448 K. Then the decomposition reaction of δ-HMX is accelerated as the temperature of the explosive is raised. Ignition did not occur until the temperature reached 551 K.

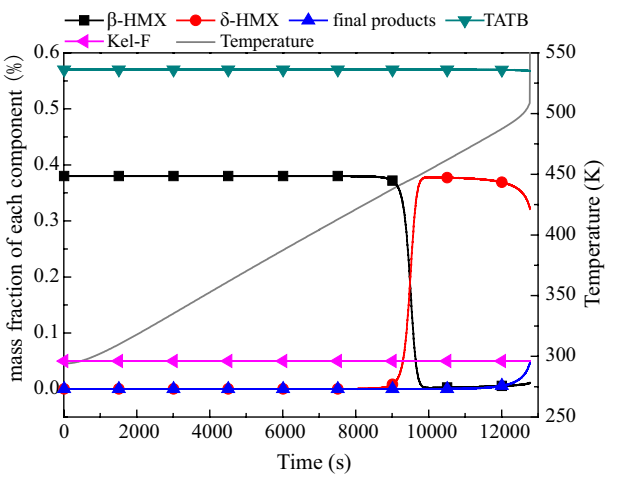

(A) PBXC-10

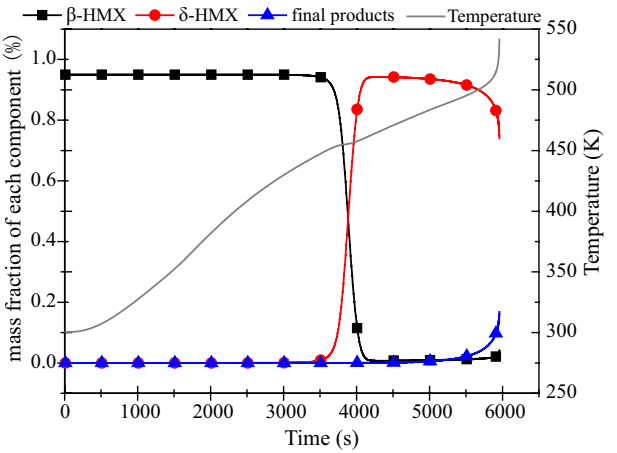

(B) JO-8

Figure 12. Calculated temperatures and mass fractions of PBXC-10 and JO-8.

In order to determine the effect of component content on the ignition time of mixed explosives, the four mixed explosives in Table 9 were calculated for different initial temperatures. The chemical kinetics parameters for HMX and TATB are listed in Table 2 and Table 3. The binder was treated as inert material. The simulations of the thermal explosion were performed for four different initial temperatures. The change in ignition times with different mixed explosives are plotted in Figure 13. It can be seen that the times to ignition for explosive A are generally longer than those containing HMX at the same temperatures, because TATB is more thermally stable than HMX, and TATB absorbs some of the HMX decomposition energy as it decomposes. The times to ignition for explosive D are the shortest overall. From the results of the computations it is also noticed that the ignition times of explosives B, C and D are nearly the same, at the temperatures of 533 K and 513 K. However, the ignition time of explosive B is much longer than explosive C and explosive D when the temperature was down to 493 K. This phenomenon can be explained by the mixed explosive compositions and the boundary temperatures. For lower temperatures, the heat generated inside can be dissipated to the outside; explosive B, containing less HMX, gives a much longer ignition time.

Table 9. Mixed explosive compositions

Explosive	Composition
Explosive A	95% TATB, 5% binder
Explosive B	57% TATB, 38% HMX, 5% binder
Explosive C	7% TATB, 87% HMX, 6% binder
Explosive D	95% HMX, 5% binder

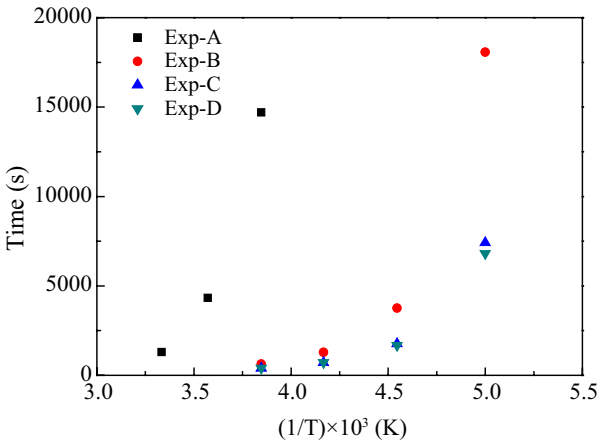

Figure 13. Relationship between ignition time of explosive and 1/T.

5 Conclusions

With the multi-point temperature cook-off test, the entire heat flow condition in the explosive is obtained from temperatures recorded from the center to the edge of the charge. The phase transition of HMX has an influence on the temperature of the explosive, especially for explosives with high HMX content. For a mixed explosive containing HMX and TATB, TATB can decrease the reaction violence in a cook-off process.

A numerical calculation method for HMX-based, mixed explosives has been considered for every component in the multi-step chemical reaction and the proportion of every component in the explosive. So the thermal decomposition reaction of HMX-based explosive can be predicted as long as the chemical kinetics model of every pure explosive and binder are known, and that does not depend on the cook-off test absolutely. It is very important for designing HMX-based mixed explosives to understand their thermal reaction characteristics beforehand.

For the mixed explosive containing HMX and TATB, most of the heat released is produced by the decomposition reaction of HMX before ignition, and the consumption of TATB and Kel-F is small. Explosives containing more TATB have longer ignition delay times.

Acknowledgements
We would like to thank the Institute of Chemical Materials of the China Academy of Engineering Physics and Xi'an Modern Chemistry Research Institute for supporting this work.

6 References

[1] Sechmit G.T., Faubion B.D., *ODTX Test Program*, MHSMP-80-48, **1980**.
[2] Hsu P.C., Hust G., Howard M., Maienschein J.L., The ODTX System for Thermal Ignition and Thermal Safety Study of Energetic Materials, *The 14th International Detonation Symposium*, April, Coeur d'Alene Resort, **2010**.
[3] Hsu P.C., Hust G., May C., Howard M., Chidester S.K., Springer H.K., Maienschein J.L., *Study of Thermal Sensitivity and Thermal Explosion Violence of Energetic Materials in the LLNL ODTX System*, LLNL-PROC-492217, Lawrence Livermore Laboratory, Livermore, **2011**.
[4] Pakulak J.M., USA Small-scale Cook-off Bomb (SCB) Test, *Minutes of 21st Department of Defense Explosives Safety Board Explosives Safety Seminar*, August, Houston, **1984**.
[5] Christian S.L., *Cook-off Modeling of PBXN-112 in a Small-scale Cook-off Bomb Using AlE3D*, California State University, Chico, **2007**.
[6] Wardell J.F., Maienschein J.L., The Scaled Thermal Explosion Experiment, *The 12th International Detonation Symposium*, August, San Diego, **2002**.
[7] Kaneshige M.J., Renlund A.M., Schmitt R.G., Erikson W.W., Cook-off Experiments for Model Validation at Sandia National Laboratories, *The 12th International Detonation Symposium*, August, San Diego, **2002**.
[8] Semenov N.N., Theories of Combustion Process, *Z. fur Physik*, **1928**, *48*, 571-582.
[9] Frank-Kamenetskii D.A., Calculation of Thermal Explosion Limits, *Acta Physicochimica U.R.S.S.*, **1939**, *10*, 365-370.
[10] McGuire R.R., Tarver C.M., *Chemical Decomposition Models for Thermal Explosion of Confined HMX, RDX, and TNT Explosives*, UCRL-84986, Lawrence Livermore Laboratory, Livermore, **1981**.
[11] Tarver C.M., Koerner J.G., Effects of Endothermic Binders on Times to Explosion of HMX- and TATB-Based Plastic Bonded Explosives, *J. Energ. Mater.*, **2008**, *26*, 1-28.
[12] Tarver C.M., Effects of Exothermic Binders on Times to Explosion of HMX Plastic Bonded Explosives, *The 14th International Detonation Symposium*, April, Coeur

d'Alene Resort, **2010**.
[13] Yoh J.J., McClelland M.A., Maienschein J.L., Wardell J.F., Tarver C.M., Simulating Thermal Explosion of RDX-based Explosives: Model Comparison with Experiment, *J. Appl. Phys*., **2005**, *97*, 1-11.
[14] Yoh J.J., McClelland M.A., Maienschein J.L., Nichols A.L., Tarver C.M., Simulating Thermal Explosion of HMX-based Explosives: Model Comparison with Experiment, *J. Appl. Phys*., **2006**, *100*, 1-9.
[15] Dickson P.M., Asay B.W., Henson B.F., Fugard C.S., Wong J., Measurement of Phase Change and Thermal Decomposition Kinetics During Cook-off of PBX 9501, *AIP Conference Proceedings*, June, Snowbird, **1999**.
[16] Perry W.L., Gunderson J.A., Dickson P.M., Application of a Reversible Four-step HMX Kinetic Model to an Impact-induced Friction Ignition Problem, *The 14th International Detonation Symposium*, April, Coeur d'Alene Resort, **2010**.
[17] Šelešovský J., Thermal Loading of Explosives − Finite Difference Method with Time Step Reduction, *J. Hazard. Mater*., **2010**, *174*, 289-294.
[18] Aydemir E., Ulas A., A Numerical Study on the Thermal Initiation of a Confined Explosive in 2-D Geometry, *J. Hazard. Mater*., **2011**, *186*, 396-400.
[19] Henson B.F., Asay B.W., Sander R.K., Son S.F., Robinson J.M., Dickson P.M., Dynamic Measurement of the HMX β-δ Phase Transition by Second Harmonic Generation, *Phys. Rev. Lett*., **1999**, *82*, 1213-1216.
[20] Land T.A., Siekhaus W.J., Foltz M.F., Beherns R. Jr., Condensed-phase Thermal Decomposition of TATB Investigated by AFM and STMBMS, *The 10th International Detonation Symposium*, July, Boston, **1993**.
[21] Dong H.S., Zhou F.F., *Performance of High Explosives and Related Materials*, Science Press, Beijing, **1989**.